Ultramicroscopy 111 (2011) 1659–1669

Contents lists available at SciVerse ScienceDirect

Ultramicroscopy

journal homepage: www.elsevier.com/locate/ultramic

Interlaboratory round robin on cantilever calibration for AFM force spectroscopy

Joost te Riet [a,b], Allard J. Katan [c,1], Christian Rankl [d], Stefan W. Stahl [e], Arend M. van Buul [f], In Yee Phang [g,h,2], Alberto Gomez-Casado [i], Peter Schön [g], Jan W. Gerritsen [a], Alessandra Cambi [b], Alan E. Rowan [f], G. Julius Vancso [g,h], Pascal Jonkheijm [i], Jurriaan Huskens [i], Tjerk H. Oosterkamp [c], Hermann Gaub [e], Peter Hinterdorfer [j], Carl G. Figdor [b], Sylvia Speller [a,*]

[a] Scanning Probe Microscopy, Radboud University Nijmegen, P.O. Box 9010, 6500 GL Nijmegen, The Netherlands
[b] Tumor Immunology, Radboud University Nijmegen Medical Centre, P.O. Box 9101, 6500 HB Nijmegen, The Netherlands
[c] Kamerling Onnes Laboratory, Leiden University, P.O. Box 9504, 2300 RA Leiden, The Netherlands
[d] Agilent Technologies Austria GmbH, Altenbergerstr. 52, A-4040 Linz, Austria
[e] Applied Physics, Ludwig-Maximilian-University Munich, Amalienstr. 54, 80799 München, Germany
[f] Molecular Materials, Radboud University Nijmegen, P.O. Box 9010, 6500 GL Nijmegen, The Netherlands
[g] Materials Science and Technology of Polymers, University of Twente, P.O. Box 217, 7500 AE Enschede, The Netherlands
[h] Dutch Polymer Institute, P.O. Box 902, 5600 AX Eindhoven, The Netherlands
[i] Molecular Nanofabrication, University of Twente, P.O. Box 217, 7500 AE Enschede, The Netherlands
[j] Institute for Biophysics, University of Linz, A-4040 Linz, Austria

ARTICLE INFO

Article history:
Received 13 July 2011
Received in revised form
12 September 2011
Accepted 16 September 2011
Available online 24 September 2011

Keywords:
Atomic force microscopy
AFM force spectroscopy
Spring constant
Round robin experiment
Cantilever calibration

ABSTRACT

Single-molecule force spectroscopy studies performed by Atomic Force Microscopes (AFMs) strongly rely on accurately determined cantilever spring constants. Hence, to calibrate cantilevers, a reliable calibration protocol is essential. Although the thermal noise method and the direct Sader method are frequently used for cantilever calibration, there is no consensus on the optimal calibration of soft and V-shaped cantilevers, especially those used in force spectroscopy. Therefore, in this study we aimed at establishing a commonly accepted approach to accurately calibrate compliant and V-shaped cantilevers. In a round robin experiment involving eight different laboratories we compared the thermal noise and the Sader method on ten commercial and custom-built AFMs. We found that spring constants of both rectangular and V-shaped cantilevers can accurately be determined with both methods, although the Sader method proved to be superior. Furthermore, we observed that simultaneous application of both methods on an AFM proved an accurate consistency check of the instrument and thus provides optimal and highly reproducible calibration. To illustrate the importance of optimal calibration, we show that for biological force spectroscopy studies, an erroneously calibrated cantilever can significantly affect the derived (bio)physical parameters. Taken together, our findings demonstrated that with the pre-established protocol described reliable spring constants can be obtained for different types of cantilevers.

1. Introduction

The Atomic Force Microscope (AFM) is a sensitive force probe [1] with a resolution in the picoNewton (pN) range, allowing characterization of inter- and intra-molecular forces. The study of single molecule bond dynamics by AFM, known as AFM force spectroscopy, is widely used to investigate biological and chemical interactions, providing insight into their intra-molecular energy landscapes [2,3]. In 1994, individual ligand–receptor interactions between avidin and biotin were measured for the first time [4,5]. Since then, force spectroscopy has been used to study, e.g., DNA structure [6,7], unfolding of native proteins [8,9], polymers [10], covalent bonds [11], rupture of supramolecular bonds [12], and cell adhesion [13,14]. All these force measurements rely on the use of well calibrated cantilevers, i.e., to know the absolute spring constant allowing one to quantify the forces. In addition, many other AFM applications such as nanostructuring [15], elasticity mapping [10,16], and static as well as resonant imaging modes [17] depend on an accurately determined spring constant in order to quantify the physical forces probed.

* Corresponding author.
E-mail address: s.speller@science.ru.nl (S. Speller).
[1] Present address: Lawrence Berkeley National Laboratory, CA, USA.
[2] Present address: Institute of Materials Research and Engineering, Singapore, Singapore.

0304-3991/$ - see front matter © 2011 Published by Elsevier B.V.
doi:10.1016/j.ultramic.2011.09.012

Over the last decades, several methods have been proposed to determine AFM cantilever spring constants that can be grouped into three categories. Dimensional modeling methods require precise knowledge of the cantilever dimensions and material properties to calculate the spring constant [18–20]. Static deflection methods use glass fibers [21,22], reference cantilevers [23,24], electrostatic forces [25], or a piezosensor [26] to determine the spring constant by loading the cantilever with a known static force. Finally, there are different dynamic deflection methods that relate the spring constant to the cantilever's resonance behavior, such as the Cleveland method [27], the thermal noise method [28], the Sader method [29,30] and laser Doppler vibrometry [31].

All these methods have previously been discussed and compared with each other [31–35]. Specifically, the thermal noise method – based on statistical mechanics – and the Sader method – based on fluid dynamics theory – have been frequently investigated and have the highest application potential, as documented by their implementation in commercial AFMs. Relatively widespread use of these approaches is mainly related to the following advantages: (i) the calibration of the cantilever is performed in situ; (ii) both methods are independent on the cantilever's material or coating; (iii) and they are (largely) nondestructive and noninvasive for the cantilevers. In addition, (iv) the AFM systems used need minimal hard- and software requirements; and finally, (v) both methods are quick and easy to learn. However, upon applying the thermal noise method, it is important to use the accurate correction factors that are described in the literature [32,36,37]. These factors mainly concern differences between rectangular versus V-shaped cantilevers, the cantilever's complex spring behavior, and the AFM's detection scheme.

In earlier studies, the implementation of the thermal noise and Sader methods were described, especially paying attention to technical and theoretical aspects [32,33], demonstrating the calibration of rectangular-shaped cantilevers within a wide spring constant range (0.1–20 N/m) [32]. However, in those studies V-shaped cantilevers were not calibrated. Other reports addressing V-shaped cantilevers did not consider the Sader method [34,38]. In view of the increasing importance of deriving quantitative forces for AFM force spectroscopy, a comparison between the methods addressing cantilevers frequently used in these studies – soft (<0.05 N/m) and V-shaped – has become necessary.

The aim of our study was to investigate potential differences of spring constants calibrated on different (commercial) instruments and in different laboratories, particularly paying attention to practical aspects of cantilever calibration. The experiments described in this article were performed sequentially, as a round robin experiment. In particular, we investigated the accuracy of the thermal noise and direct Sader method by calibrating cantilevers on different AFM systems operated by experienced users in different labs all using the same calibration protocol. Furthermore, two indirect methods by Gibson and Sader [29,39], which relate the spring constant of the rectangular to the V-shaped cantilever on one chip, were considered as alternatives. Finally, we discuss the effect of an incorrectly determined spring constant on the measured forces and micromechanical properties of a biological ligand–receptor bond. We conclude our study by proposing a practical and reliable calibration protocol to obtain reliable spring constants for different types of cantilevers.

2. Materials and methods

2.1. Round robin experiment

The round robin study was set up as a collaboration between eight laboratories from three countries. In these labs different commercial and custom-built AFMs were used to study the same 30 cantilevers on 10 different chips, which were sent around from one lab to the next to sequentially determine their spring constants. The calibrations were performed by experienced users of the AFM systems according to a protocol pre-established by all participants, see Appendix A.

2.2. Instruments

Ten different AFMs were used, of which the description, abbreviation, and location, are given in Table 1. We include a symbol (Roman numerals) to designate the AFMs throughout the study. A brief description of the instruments is given below, detailed information on the software used, the temperature, etc., can be found in Table S1 (Supplementary material).

Multimode Nanoscope IIIa (Veeco, Santa Barbara, CA, USA). Calibrations on the Nijmegen [I] and Enschede [III] AFM systems were performed on thermal noise data sampled at a rate of 62.5 kHz. In detail, false engage images (512×512) of trace and retrace at a line rate of 61 Hz were exported including time series of the successive scan lines, and a power spectral density (PSD) analysis was performed on these data, to obtain all calibration parameters by a fit for further analysis. Calibrations on the Leiden system [II] were performed by routing the deflection data from the Signal Access Module to a 16 bit DAQ card (USB 6152, National Instruments) and recording them at a sample rate of 1.25 MHz. Spectra were calculated from these data during acquisition using custom-written LabView software.

Multimode Nanoscope IV (Veeco). Calibrations on the Nijmegen system [IV] were performed by measuring the thermal noise data at a sampling rate of 62.5 kHz via the Thermal Tune box in the software. Thermal noise spectra were exported and analyzed.

Multimode Nanoscope IVa (Veeco). Calibrations on the Enschede PicoForce system [V] were performed by measuring the thermal noise data at a sampling rate of 62.5 kHz via the Thermal Tune box in the software. InvOLS (inverse optical lever sensitivity (nm/V); also known as deflection sensitivity [40]) measurements were performed

Table 1
Outline of AFM systems used.

Symbol	Abbreviation	System	Location
I	NS IIIa	Veeco Multimode Nanoscope IIIa	Nijmegen (NL)
II	NS IIIa	Veeco Multimode Nanoscope IIIa	Leiden (NL)
III	NS IIIa	Veeco Multimode Nanoscope IIIa	Enschede (NL)
IV	NS IV	Veeco Multimode Nanoscope IV	Nijmegen (NL)
V	NS IVa	Veeco Multimode Nanoscope IVa	Enschede (NL)
VI	NS V	Veeco Multimode Nanoscope V	Nijmegen (NL)
VII	JPK	JPK NanoWizard I	Nijmegen (NL)
VIII	Agilent 5500	Agilent 5500	Linz (A)
IX	CB	Custom-built based on Asylum MFP-3D	Munich (D)
X	CB	Custom-built	Leiden (NL)

with closed *z*-loop. Thermal noise spectra were exported and analyzed.

Multimode Nanoscope V (Veeco). Calibrations on the Nijmegen system [VI] were performed by measuring the thermal noise data at a sampling rate of 200 kHz via the Thermal Tune box in the software, in which also the thermal noise spectra were analyzed via the Liquid (SHO) fitting procedure.

JPK NanoWizard I (JPK, Berlin, Germany). Calibrations on the Nijmegen system [VII] were performed by measuring the thermal noise at a sampling rate of 152 kHz via the JPK software, in which also the thermal noise spectra were analyzed.

Agilent 5500 (Agilent, Chandler, AZ, USA). Calibrations on the Linz system [VIII] were performed by obtaining the thermal noise data at a sampling rate of 220 kHz. Spectra generation and curve fitting was performed by a custom written software in MATLAB (The Mathworks, Natick, MA, USA).

Custom-built system (CB) with Asylum MFP-3D controller (Asylum Research, Santa Barbara, CA, USA). Calibrations on the Munich system [IX] were performed by obtaining the thermal noise data at a sampling rate of 5 MHz. Generation of spectra and curve fitting were performed in Igor 5.03 (Wavemetrics Inc., OR, USA) with software packages provided by Asylum Research.

Custom-built system. Thermal noise spectra on the Leiden system [X] were acquired on a high-speed digitizer with built-in FFT calculation (National Instruments PCI 5122), using a sample rate of 10 MHz and a frequency resolution of 4 Hz.

Note that before the experiments, the *z*-calibration of all AFMs was checked using a calibration grid, or via interference measurements (for system IX).

2.3. Cantilevers

The cantilevers used in this round robin study were 5 MLCT-AUHW (Veeco) and 5 MSCT-AUHW (Oxide-Sharpened MLCTs, Veeco). The nominal – i.e., given by the manufacturer – spring constants are given in Table 2. The cantilever dimensions were measured by a JEOL scanning electron microscope (SEM; JSM-6301F) using a dedicated internal calibration grid to relate the dimensions measured by the SEM (Table 2). These dimensions were determined once and used throughout the whole round robin study.

Cantilevers were cleaned once before the calibration series by rinsing them three times with chloroform (Sigma-Aldrich, St. Louis, MO, USA) and subsequently with $>98\%$ ethanol (Sigma). Then the cantilevers were UV-cleaned for 20 min, rinsed with ethanol, MQ water and as a last step with ethanol. Finally, the cantilevers were dried in a N_2 flow.

2.4. The thermal noise method

In this method the cantilever is treated as a simple harmonic oscillator. The equipartition theorem, which says each mode of the cantilever on average contains an amount of energy $1/2k_BT$, is then used to find the cantilever spring constant k by relating the thermal (i.e., Brownian) motion of the cantilever's fundamental mode to its thermal energy [28]:

$$k = \frac{k_B T}{\langle z_c^2 \rangle} \tag{1}$$

where k_B is the Boltzmann constant, T the temperature, and $\langle z_c^2 \rangle$ the mean square displacement of the cantilever. Later studies pointed out that two corrections were necessary [36,37]. The first correction takes into account the fact the energy of the fundamental oscillatory mode of a cantilever spring is not simply $1/2k_BT$, where x is the measured displacement at its end, but must be calculated in terms of an integral of the elastic energy over the cantilever. Correction factors of 0.971 and 0.965 were found for rectangular [36] and V-shaped cantilevers [37], respectively. A second, more significant correction takes into account the optical lever detection scheme [36] in which the *angular* changes of the cantilever are measured rather than the absolute deflection. Since the curvature profile of a freely oscillating cantilever (used to collect the thermal noise data) differs from that of a supported one (used to measure InvOLS) the measured 'displacement' is corrected. These also depend on the bending mode of the cantilever, for the primary mode the following formula was derived (with $C=0.817$ or 0.764 for rectangular and V-shaped cantilevers, respectively) [36,37]:

$$k = C\frac{k_B T}{\langle z_1^{*2} \rangle} \tag{2}$$

where $\langle z_1^{*2} \rangle$ represents the 'apparent' cantilever displacement measured by the optical lever scheme of the primary oscillation mode.

Further corrections were suggested, e.g., taking into account the finite spot size, the cantilever size, and the laser spot position on the cantilever [40,41]. However for cantilevers longer than 100 μm used in AFMs with a laser spot size smaller than 20 μm and V-shaped cantilevers (i.e., such as is the case in our study) these corrections are insignificant.

To determine $\langle z_1^{*2} \rangle$ of (2) the thermally driven oscillations of the cantilever are collected over time, followed by a power spectral density (PSD) analysis to generate a thermal spectrum. The fundamental resonance peak is then fitted to a simple harmonic oscillator (SHO) model for the power [42]:

$$P(f) = y_0 + \frac{A_0 f_R^4}{(f^2 - f_R^2)^2 + ((f f_R)/Q)^2} \tag{3}$$

where y_0 is the power of the white noise baseline, A_0 the zero frequency power, f_R the resonance frequency, and Q the quality factor. (We note that for highly damped systems, $Q \leq 10$ as for example in liquid, an adapted SHO fit should be used) [38]. The spring constant is then calculated by taking $\langle z_1^{*2} \rangle$, which represents the area under the curve of the SHO fit, as [32]

$$\langle z_1^{*2} \rangle = \int_{f=0}^{\infty} P(f) df \tag{4}$$

with $P(f)$ from (3), for (2) this results in:

$$k = \frac{2Ck_B T}{\pi A_0 f_R Q} \tag{5}$$

2.5. The Sader method

With the direct Sader method the spring constant of a rectangular cantilever is determined using its plan-view dimensions, the density of the medium ρ, and viscosity of the medium η in which they are measured, and the corresponding resonance frequency f_R and quality factor Q [29]. The thickness t of the

Table 2
Dimensions of the cantilevers.[a]

Cantilever	L (μm)	b (μm)	d (μm)	θ (°)	k_{nom} (pN/nm)
B_{MLCT}	203.8	20.38	n/a	n/a	20
C_{MLCT}	324.2	20.81	226.6	18.6	10
D_{MLCT}	219.6	20.26	154.9	18.6	30
B_{MSCT}	203.3	20.12	n/a	n/a	20
C_{MSCT}	321.4	21.24	222.1	18.6	10
D_{MSCT}	217.6	21.05	153.0	18.6	30

[a] Given dimensions are those determined of three randomly chosen cantilevers from one wafer.

cantilever is not needed. Typically the Sader method is applied in air, in which $Q > 10$. Additionally, the length to width ratio should be $L/b > 3$ [43]. By fitting the thermal spectrum of a rectangular cantilever with the SHO model (3), f_R and Q are determined. (For liquid see Ref. [38]). The spring constant can then be described by [29]

$$k = 7.5246\rho b^2 L\Gamma_i(\mathrm{Re})f_R^2 Q \tag{6a}$$

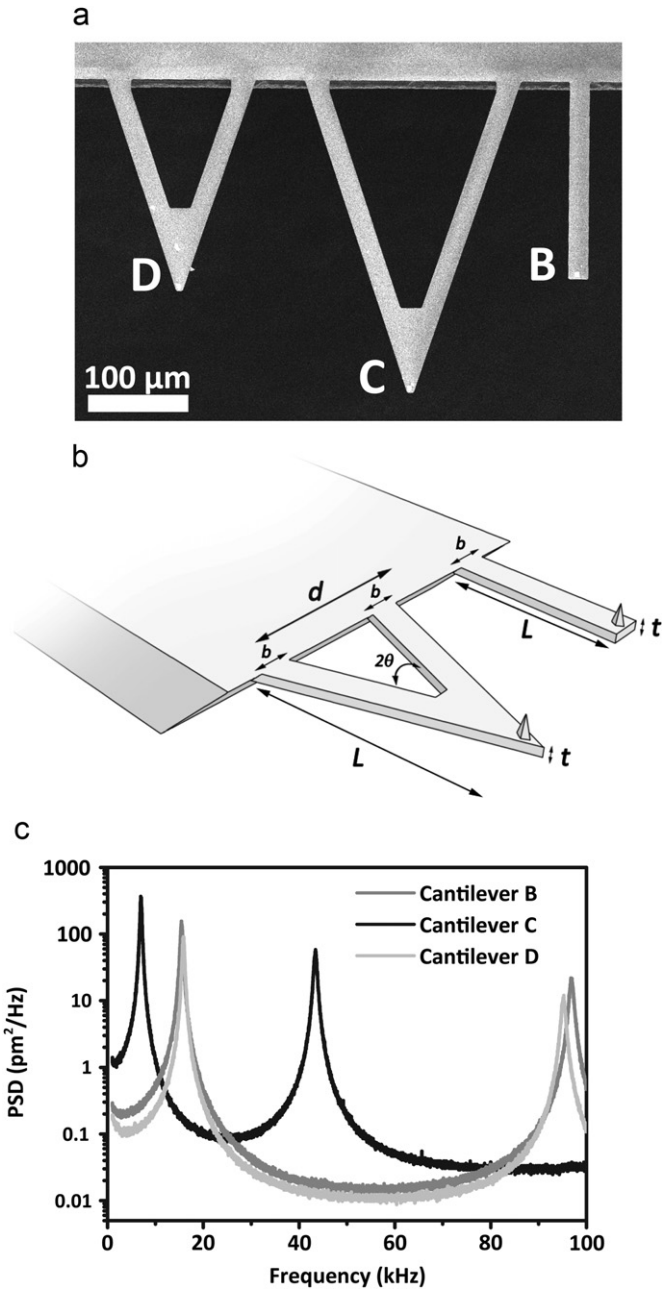

Fig. 1. Characteristics of the three types of cantilevers studied. (a) SEM image of rectangular cantilever B and V-shaped cantilevers C and D on a MSCT chip. (b) Scheme of a rectangular and V-shaped cantilever with the symbols for the dimensions as used throughout the study. (c) Thermal noise spectra of cantilevers B, C, and D on chip MLCT1 as determined with AFM system VI at a sampling rate of 200 kHz. The primary and secondary thermal noise peaks are visible for all three cantilevers. In the spectra the white noise level is low, but shows a $1/f$ noise floor. The resonance frequencies and quality factors of the primary peaks are f_R=14.5, 6.3, and 14.5 kHz and Q=23.1, 14.9, and 25.6 for cantilevers B, C, and D, respectively.

with

$$\mathrm{Re} = \frac{\pi\rho b^2 f_R}{2\eta} \tag{6b}$$

where b is the width of the cantilever, L the length of the cantilever (see Fig. 1b), and Γ_i the imaginary part of the hydrodynamic function [44].

This model is valid for any rectangular cantilever; for V-shaped cantilevers it is necessary to determine the individual dynamical response of each cantilever. This method is described by Sader et al. [30]. In short, the response of the resonance frequency and damping factor are measured according to the Reynolds number Re, which is varied by changing the air pressure. In their study formulas are derived for the V-shaped cantilevers C and D from a MSCT/MLCT chip, which are the type of cantilevers studied in this paper [30]. The formulas for cantilever type C and D are, respectively

$$k = 140.94\rho b_C^2 L_C \mathrm{Re}^{-0.728+0.00915\ln\mathrm{Re}} f_R^2 Q \tag{7a}$$

$$k = 117.25\rho b_D^2 L_D \mathrm{Re}^{-0.700+0.0215\ln\mathrm{Re}} f_R^2 Q \tag{7b}$$

with b_C or b_D the width of one of the two cantilever beams (Fig. 1b), L_C or L_D the length of the cantilever and the Reynolds numbers as in (6b).

2.6. Cantilever tilt

In an AFM cantilevers are usually mounted at a small angle with respect to the horizontal (scan) direction to prevent contact between the cantilever chip and the sample. Different AFMs have different tilt angles α varying from 6–12° (see Table S1). Therefore, it is convenient to compare intrinsic spring constants, rather than tilt-dependent effective values [45]. Intrinsic values are explicitly provided by the Sader method, while effective values are obtained by the traditional implementation of the thermal noise method. Thus, this implies that these spring constants should be corrected by a factor of $\cos^2\alpha$ as described in Ref. [45]. The relation between the effective (thermal noise) and intrinsic (Sader) spring constants is

$$k_{effective} = \frac{k_{intrinsic}}{\cos^2\alpha} \tag{8}$$

An additional correction is needed if the tip protruding from the cantilever is long compared to the cantilever's length [45]. However, this correction is small in most cases, including the present study.

3. Results and discussion

3.1. Physical characteristics of the cantilevers used for calibration

Tested cantilevers are of the MSCT/MLCT-type—one of the most applied types of cantilevers in AFM force spectroscopy studies, due to their low spring constant, uniformity, robustness, and affordability. We choose to study only the softest cantilevers of the chip, i.e., B, C, and D. The dimensions of cantilevers B, C and D, needed for the Sader method, were determined by scanning electron microscopy (SEM). In the SEM image (Fig. 1a) the arrangement of cantilevers B (rectangular), C and D (V-shaped) is shown. The dimensions of each cantilever on three MLCT- and three MSCT-cantilever chips were determined and the mean values are given in Table 2 (see Fig. 1b for labels). The differences between the manufacturer's specifications and the measured dimensions of the cantilevers were smaller than $\pm 1.9\%$ for length and $\pm 7.9\%$ for width. Furthermore, cantilevers from the MLCT and MSCT chips have comparable sizes,

which only vary ±3.9% in width similar to the accuracy of the SEM measurements (±3.3%). Thus, it can be concluded that the manufacturer's nominal dimensions in this specific case are in good agreement with the measured ones. However, we observed that nominal values provided by manufacturers are, in general, insufficiently accurate (±10–25%). Therefore, a check of the dimensions is always recommended.

Another important parameter for the implementation of both methods is temperature, which influences the thermal fluctuations of the cantilever. We found that the temperature, measured at the location of the cantilever in its holder in a working AFM, was usually higher (up to 6 K) than room temperature. Based on Eq. (5), neglecting this temperature difference would imply a systematic error of ~2%. Therefore, actual (measured) temperatures were used in the present study.

3.2. Calibration of the cantilever spring constant by the thermal noise method

Cantilevers are calibrated with the thermal noise method using the pre-established protocol as given in the Appendix A. After InvOLS measurements, thermal noise spectra were obtained and the fundamental resonance peak was fitted with the SHO model (Eq. (3)). Thereby, the resonance frequency f_R, the quality factor Q, the zero frequency power A_0, and the power of the white noise baseline y_0 were obtained (Fig. 1c).

The spring constant of the longest type of cantilevers (C-type) was calculated with Eq. (5) using the derived parameters f_R, Q and A_0. We decided not to calibrate the shorter B- and D-type cantilevers with the thermal noise method to prevent damage of the longer C-type cantilever. This damage might occur when the InvOLS of the shorter cantilevers is measured and the longer C-type cantilever would come into full contact with the substrate. In Fig. 2d, the result is shown of calibrating 10 C-type MLCT/MSCT-cantilevers (see Table S2d for corresponding values). In both Fig. 2d and Table S2d, the intrinsic spring constants are presented, i.e., corrected for cantilever tilt by Eq. (8). In Fig. 2d only the spring constants determined on AFMs [I–IX] are shown. On system X, which was optimized for fast sampling, it was impossible to perform calibrations with the thermal noise method; due to the small z-range of the piezo scanner, the required InvOLS could not be determined as the cantilever did not detach from the substrate, due to strong electrostatic interactions.

When comparing the results obtained on the MLCT and MSCT cantilevers, cantilevers from the same wafer, i.e., MLCT 1–5, MSCT

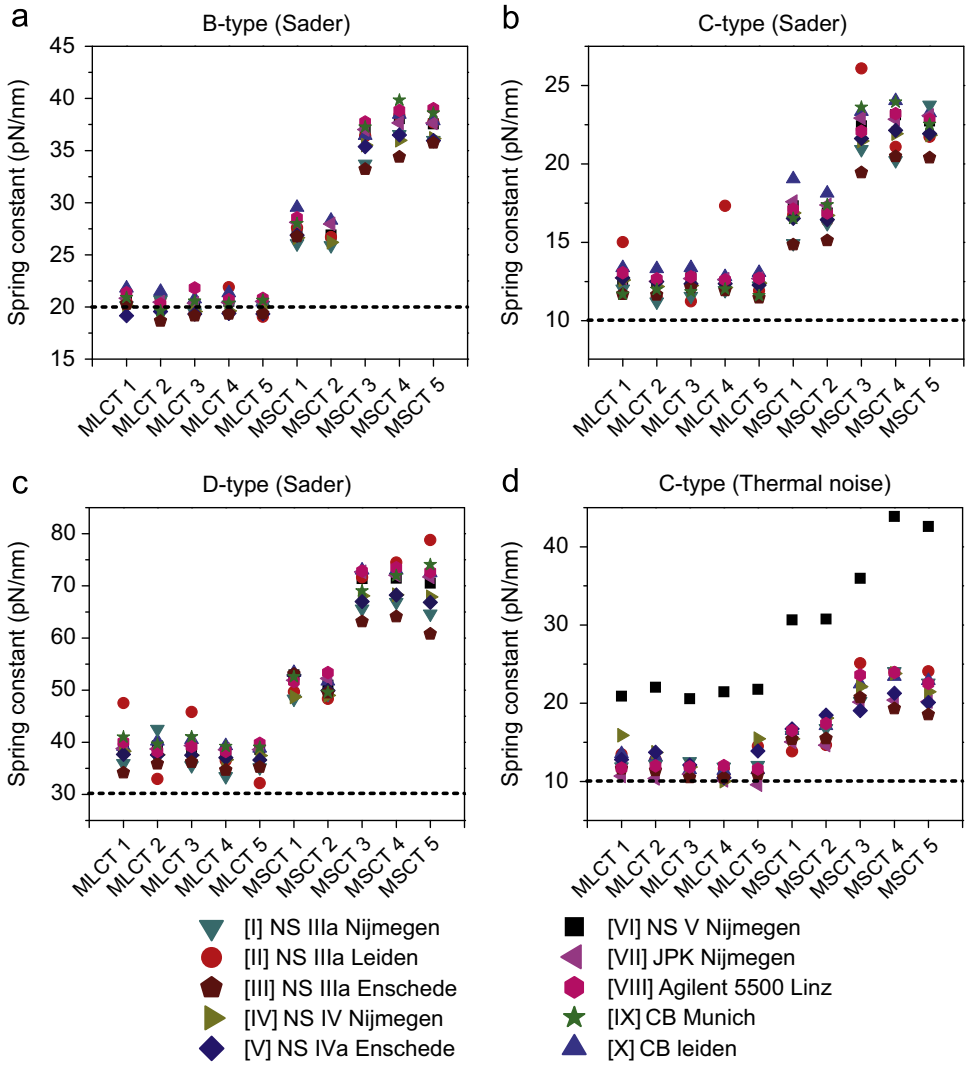

Fig. 2. Cantilever spring constants as determined on different AFMs with the thermal noise and Sader methods. The mean spring constants ($N=5$) determined for calibrating cantilevers of MLCT and MSCT chips on 10 AFM systems. (a) Using the Sader method to calibrate cantilevers of the B-type, (b) the C-type, (c) and the D-type. (d) Calibrating the C-type cantilevers with the thermal noise method. The different AFMs are represented by different symbols. The cantilever spring constants as given by the manufacturer are indicated by dotted lines (20, 10, and 30 pN/nm).

1–2, and MSCT 3–5, were found to nearly exhibit the same spring constants, within an error of ~4% (Fig. 2d). However, cantilevers from these different chips vary substantially in spring constants. Moreover, if compared to the nominal value given by the manufacturer (10 pN/nm) the measured values of cantilevers MSCT 3–5 are more than double. This example illustrates the importance of manual cantilever calibration instead of simply taking the provided spring constant, which could lead to errors up to ~125%.

3.3. Calibration of the cantilever spring constant by the Sader method

In order to apply the (direct) Sader method, the resonance frequency f_R and the quality factor Q of the cantilevers must be determined first. These are obtained by fitting the thermal noise spectrum of the cantilever. From the obtained parameters and the dimensions of the cantilever (Table 2), the spring constant is calculated using Eqs. (6) or (7).

For the C-type cantilevers the spring constants are instantly calculated from the earlier obtained thermal noise method data and are shown in Fig. 2b and Table S2b. The thermal noise spectra of cantilevers B and D were determined in a similar way, only the laser was re-aligned to these cantilevers, which were kept at all times well above the substrate. The corresponding spectra were analyzed to obtain f_R and Q. As A_0 is not needed for further analysis, it was not necessary to measure the InvOLS in this case. In this way, it is now possible to also calibrate the shorter cantilevers on the chip. The spring constants of cantilevers B and D were determined on all 10 AFMs and are shown in Fig. 2a and c and Table S2a and c, for the B- and D-type of the 10 MLCT/MSCT-chips, respectively. The obtained values are less scattered, and have the same mean value as those of the thermal noise method.

3.4. Comparison of the results obtained with the Sader method on different AFMs

To gain a better insight into the performance of every AFM alone and to be able to compare them with each other, each measurements was normalized to the mean value obtained for the corresponding cantilever using AFM systems [IV–X] (Table 3). We excluded the spring constants obtained on the NS IIIa systems [I–III] in calculating the mean spring constant, because of a high amount of outliers.

Table 3
Spring constants of the cantilevers (pN/nm).[a]

Chip name	*B-type*	*C-type*			*D-type*		
	k_{mean}	k_{mean}	Indirect Sader	Gibson	k_{mean}	Indirect Sader	Gibson
MLCT 1	20.7	12.9	9.9	9.9	39.1	31.0	30.8
MLCT 2	20.3	12.8	9.7	9.6	38.8	30.3	30.3
MLCT 3	20.3	12.8	9.8	10.1	39.1	30.4	31.0
MLCT 4	20.3	12.5	9.8	9.8	38.2	30.4	30.3
MLCT 5	20.3	12.6	9.7	9.8	38.4	30.4	30.0
MSCT 1	27.9	17.3	13.9	14.1	52.0	44.7	41.5
MSCT 2	27.3	16.9	13.6	13.6	51.0	43.8	40.7
MSCT 3	36.6	22.2	18.3	17.8	70.6	58.7	55.7
MSCT 4	37.9	23.0	18.9	18.3	71.2	60.8	58.2
MSCT 5	37.5	22.7	18.7	18.4	70.9	60.2	56.7

[a] Mean values are given of the spring constants obtained on AFMs [IV–X] with the Sader method in 5 subsequent measurements (see also Table S2 for the values obtained on all instruments and with both methods).

The normalized spring constants obtained with the Sader method for the rectangular B-cantilevers are relatively uniform for all AFM systems (Fig. 3a). The observed variation is only 1–3% for every single AFM, and the overall variation in normalized spring constants of all instruments is within a ±6% error in relation to the overall mean cantilever spring constant. For the V-shaped cantilevers of the C- and D-type, the results are in good agreement with the mean cantilever spring constant except for the results obtained on the three NS IIIa systems (Fig. 3b and c). Keeping the results on these three systems out of consideration for a moment, we observe a variation in mean spring constants for each individual AFM of ±2% for C-type as well as for D-type cantilevers. This is similar to the B-type cantilevers. Taking the results of all these AFMs [IV–X] together, a deviation of ±5% is found for both the C- and D-type cantilevers.

For the normalized spring constants obtained on the NS IIIa systems [I–III], however, we observe a systematic error of −4% (±7%) (Fig. 3b and c). This suggests that the obtained spring constants are underestimated and less accurate, especially on system II. An explanation could come from the different way of acquiring the thermal noise data on the NS IIIa systems [I–III] with respect to AFMs IV–IX. Thermal noise data on systems I&III, and II were acquired internally and externally, respectively, and were analyzed off line. As it is not a priori clear how many samplings are necessary to get a spectrum with an acceptable signal-to-noise ratio, the acquisition time may have been too short, resulting in a less accurate fit of the thermal noise spectra.

3.5. Comparison of the results obtained with the thermal noise method on different AFMs

The data obtained with the thermal noise method indicate that the mean spring constants determined for the C-type cantilevers are equal to those determined by the Sader method (Fig. 3d). However, for most of the AFMs, the distributions in values obtained are significant (±3 to ±11%). Having a closer look at the calibrations with the NS IIIa systems I–III, the spring constants are more accurately determined with the thermal noise method than with the Sader method. However, spring constants measured on AFMs V, VI, and VIII are systematically off from the mean. For systems V and VIII this can most likely be attributed to the calibration of the piezo-scanner. Afterwards checking the calibration with another grid, we observed that the given depth of the grid used before deviated from the actual value. An error of ±5% herein, which is reasonable from our own observations, leads to an error in the spring constant of ±10% as the calibration error scales quadratically with the depth. Another cause for the observed higher variations might be static interactions due to charging under low humidity. Actually, the soft C-cantilevers hardly got off the substrate during the InvOLS measurement, leading to non-ideal force curves in which the InvOLS is under- or overestimated. The accuracy of the thermal noise method determined in this study agrees well with the estimated error of ±8% reported by Ohler [33], which they mainly attribute to the error in the InvOLS. In addition to that error, we found that also the error in z-calibration of the AFM has to be taken into account and advise to calibrate it with great care to avoid error propagation.

Still remains the overestimation by ~74% of spring constants calibrated in system VI with the thermal noise method. In fact, on this system high quality calibrations could be performed with the Sader method (Fig. 3a–c). Moreover, this system was calibrated with the same calibration grid as systems I, IV, and VII, suggesting that something completely different is the cause of this overestimation. Most likely, a defect in the implemented hard- or software related to the InvOLS measurements gives rise to this error, for which the system is under revision. Additional information

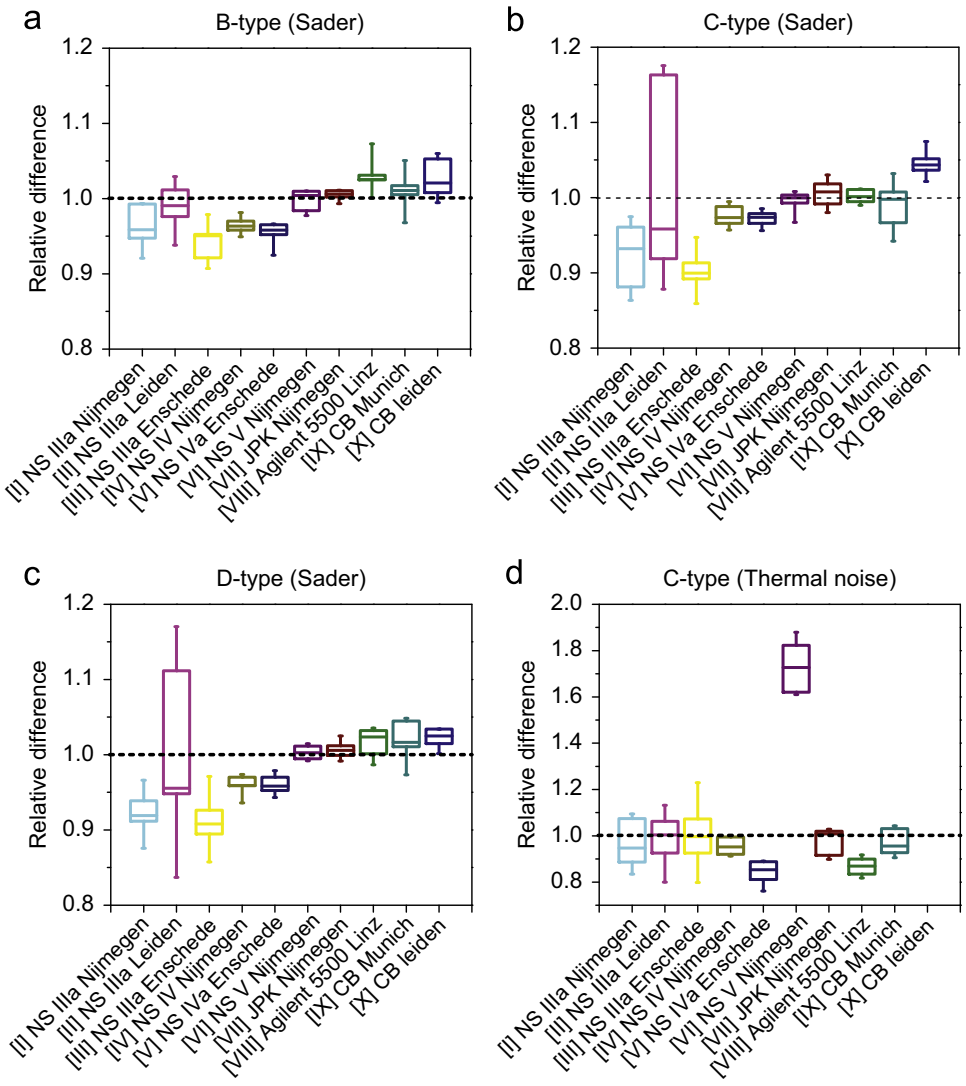

Fig. 3. Comparison of the accuracies of the AFMs. Box plot in which the accuracies of 10 AFMs are compared by normalizing each of the measured cantilever spring constants to the mean spring constant found for systems [IV–X] by the Sader method. The normalized value is set to 1 and is indicated by the dotted line in all plots. The accuracy of the systems found by applying the Sader method is plotted in, (a) in the case of the B-type, (b) C-type, and (c) D-type. (d) The accuracy of calibrating the C-type cantilever by the thermal noise method. The borders of the boxes represent the 25–75% levels, the line in the box the median and the whiskers the 10–90% levels. Note the difference in scale.

on this issue can be found on http://wiki.science.ru.nl/spm/note_calibration.

In conclusion, the above described cases of systems V, VI, and VIII nicely illustrate another interesting finding from our round robin experiment. The comparison with the other systems revealed systematic errors on these systems, which were not foreseen. Therefore, we recommend users to check consistency for the cantilever calibration on an AFM with more than one method to verify the evaluation implemented in the instrument.

3.6. The Gibson and indirect Sader method for V-shaped cantilevers

Next to direct cantilever spring constant calibration, methods also exist in which the spring constant is determined indirectly. Different theories have been described in literature, in which the spring constant of one (rectangular) cantilever can be related to the spring constant of other cantilevers located on the same chip, assuming that the material properties and thickness for each cantilever on the chip are approximately the same [29,39]. These methods are described as alternatives for the calibration of cantilevers that could not be calibrated due to technical difficulties or with differently shaped cantilevers. In our case, this implies that for the MLCT/MSCT-cantilever chips, the spring constant obtained for the rectangular cantilever B can be used to calculate the spring constant of the V-shaped cantilevers C and D on the same chip. Two different methods were selected to compare the accuracy of such indirect calibration approaches to the direct Sader method and thermal noise methods. First, we applied the indirect method described by Sader et al. [29] that combines the Euler–Bernoulli beam theory [46] for rectangular cantilevers and the parallel beam approximation (PBA) [47] for V-shaped cantilevers. This leads to the following equation for the spring constants of cantilevers C and D using that of B:

$$k_{C/D} = \frac{2k_B L_B^3 d_{C/D}}{L_{C/D}^3 b_B} \cos\theta_{C/D} \left[1 + \frac{4b_{C/D}^3}{d_{C/D}^3}(3\cos\theta_{C/D} - 2)\right]^{-1} \quad (9)$$

where $\theta_{C/D}$ is the half angle in between the two beams of the V-shaped cantilevers C or D and $d_{C/D}$ the full width at the base of the cantilevers (Fig. 1b). Secondly, the indirect method described by Gibson et al. [39] was used, in which the spring constants of two

cantilevers (k_1 and k_2) are related via

$$k_1 = \frac{n_1 A_1}{n_2 A_2}\left(\frac{f_1}{f_2}\right)^2 k_2 \quad (10)$$

where, n_1/n_2 is the ratio between the shape factors of the cantilevers, A_1/A_2 between their areas and f_1/f_2 between their resonance frequencies. The SEM images (Fig. 1a) were used to determine the areas of the cantilevers. The shape factors were derived using data from Sader et al. [48], from cantilever dimensions (Table 2) and a Poisson ratio of 0.24. For cantilever C related to B, this resulted in a factor $n_C A_c/n_B A_B = 2.486$ and for cantilever D in $n_D A_D/n_B A_B = 1.467$.

Subsequently, the spring constants for the C- and D-type cantilevers were calculated by Eqs. (9) and (10) using the spring constants of the B-type obtained earlier, and are given in Table 3. The spring constants calculated with the indirect Sader method are consequently 21 ± 2% and 18 ± 3% underestimated for cantilevers C and D, respectively. In addition, the results calculated with the Gibson method are also 21 ± 2% underestimated for both C and D. However, when the similarly shaped C- and D-cantilevers are compared, the spring constants extrapolated from one to the other are well related within a ± 1% error (data not shown). One explanation for the discrepancy of ~20% between directly or indirectly obtained spring constants can be that in both indirect methods the V-shaped cantilever is considered as two beams connected under an angle, which does not account for their real shape [47]. Besides, both indirect methods assume a uniform material density of the cantilevers, although in reality they consist of stacked layers of SiN_4 and gold. Probably, corrections to (9), as for example suggested by Hazel and Tsukruk [49], would better describe V-shaped and bi-component cantilevers. In conclusion, indirect methods can only be used to calculate spring constants of cantilevers when the cantilevers have the same shape.

3.7. Biological implications for AFM force spectroscopy

The importance of accurate calibration of an AFM cantilever becomes evident when AFM Force Spectroscopy is used to study, e.g., biological receptor–ligand interactions at the single molecule and/or single cell level. Upon comparison of data from different studies, conclusions drawn on measured parameters might be wrong due to the use of an inaccurate spring constant calibration protocol. In general, these comparisons between rupture forces F_{rup} are done at a particular loading rate r_f (rate of increase in force). Furthermore, the rupture forces and loading rates are such related that data will appear as a straight line in a semi-logarithmical plot of the force spectrum vs. loading rate (Fig. 4), which is described by the Bell model [50]. In this model, the mean rupture force is given by

$$F_{rup} = \frac{k_B T}{x_\beta}\ln\left(\frac{x_\beta}{k^0_{off} k_B T}\right) + \frac{k_B T}{x_\beta}\ln(r_f) \quad (11)$$

where k^0_{off} is the dissociation rate in the absence of a pulling force, and x_β the mechanical bond-length [51,52]. The Bell model parameters k^0_{off} and x_β characterize the micromechanical properties of the ligand–receptor interaction under study and model their intra-molecular energy landscapes.

Now, if we assume an error of ± 20% in cantilever spring constant – which is reasonable based on, e.g., piezo-scanner error (± 10%), rectangular instead of V-shaped correction factor (± 7%) and ignoring correction factors (± 31%) – then the error in the observed rupture forces and loading rates is ± 20%. In the spectra, this error causes a linear shift up or down (Fig. 4; light and dark gray lines) of the data points. By fitting, we found that the error of ± 20% hardly influenced the Bell parameter k^0_{off}, but resulted in an error of ± 20% for x_β. As a consequence, we conclude that when micromechanical properties of ligand–receptors in AFM force spectroscopy are compared by means of their Bell parameters [53,54], it is safe to only compare the k^0_{off}-values from different studies, rather than the x_β-values or the rupture forces at a specific loading rate [14]. However, the use of a commonly adopted protocol with a high accuracy would make the comparison of dynamical bond parameters from different studies more trustworthy.

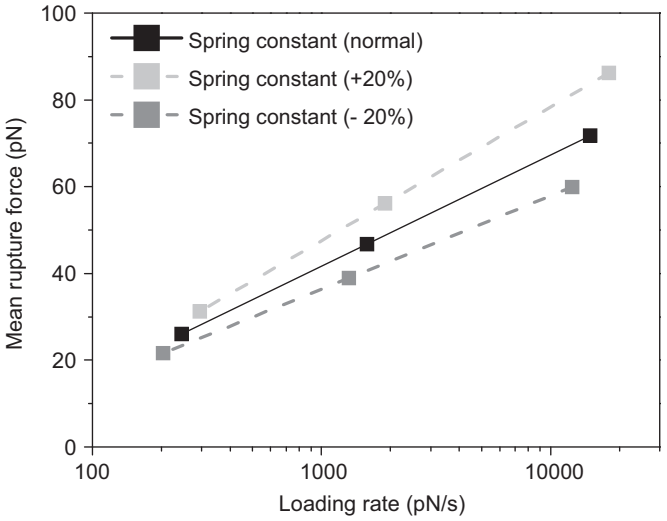

Fig. 4. Influence of under- or overestimated spring constants on the force spectrum. The relation between the mean rupture force (F_{rup}) and the loading rate (r_f) is shown in a force spectrum. Plotted is the change in obtained force spectrum by an error in spring constant of ± 20%. The data presented in this example are those acquired for the cell adhesion ligand–receptor bond ALCAM-ALCAM, as obtained in Ref. [54]. The corresponding Bell parameters are $k^0_{off} = 2.1\ s^{-1}$ and $x_\beta = 0.37$ nm. The mean rupture forces as well as the loading rates are raised or lowered according to an error of +20% (light gray) and −20% (dark gray). By fitting the newly obtained force spectra, new Bell parameters are found for these two extremes, which are $k^0_{off} = 2.1\ s^{-1}$ and $x_\beta = 0.31$ nm (for +20%) and $k^0_{off} = 2.1\ s^{-1}$ and $x_\beta = 0.45$ nm (for −20%).

Force spectroscopy, but also other scientific areas applying AFM in which quantitative measurements of forces are needed, would benefit from a uniform calibration protocol leading to an increase in accuracy of the obtained parameters, independent on AFM, cantilever, and operator. For force spectroscopy, we propose the improved, fast and versatile method described here to calibrate *in situ* functionalized AFM cantilevers, preferably applied in air, although also possible in liquids (see Appendix A). Upon application in liquid, damping of the cantilever becomes substantial and extra care should be taken in fitting and acquiring the data, especially due to commercial AFM limitations [38]. In view of our findings, a combination of the direct Sader method together with calculating the InvOLS – without getting into contact with a substrate, as described by Higgins et al. [55] – yields the best results.

4. Conclusions

In a round robin experiment we compared cantilever calibration methods on different AFMs. By comparing the results obtained on a single AFM versus the mean of 10 AFMs we found that the accuracies are ~6% vs. ~15% for the thermal noise method and ~3% vs. ~7% for the direct Sader method. This demonstrates that – even in the case of using a well-defined protocol – 'relative' errors between AFMs can be substantial.

The main cause for the error of the thermal noise method is that it suffers from systematic errors in determining the correct InvOLS, which can be mainly attributed to discrepancies in the *z*-calibrations of the AFM piezo scanner. On the other hand, the accuracy of the direct Sader method is predominantly defined by the quality of data acquisition of the thermal fluctuations of the cantilever. Another important factor is the accuracy of measuring the dimensions of the cantilever, especially the width, which normally can be measured with a ~3% accuracy by SEM. While this extra step of measuring the dimensions of every cantilever from a different wafer is intrinsic more time-consuming, clear advantages of the Sader method are its higher accuracy and the time saved by calculating instead of measuring the InvOLS.

In addition, the simultaneous implementation and comparison of both calibration methods represents a convenient and effective way to check the proper hardware and software operation of an AFM instrument. Furthermore, the 'sum' of both methods leads to a higher overall accuracy due to the elimination of systematic errors. In general, the systematic errors described in this study can be regarded as representative for errors encountered by any AFM user. It should be noted that, although this study focuses on soft cantilevers calibrated in air, the same two methods can be applied to stiffer cantilevers as well as to cantilevers in liquid.

Finally, we demonstrated that biophysical parameters obtained in force spectroscopy studies suffer from inaccurately derived spring constants. Therefore, an approved cantilever calibration protocol, as described in this report, will allow a better quantitative comparison of biophysical AFM results from different laboratories.

Acknowledgments

This study was supported by NanoNed, the Dutch nanotechnology program of the Ministry of Economic Affairs and in part financed by a BIO-LIGHT-TOUCH Grant (FP6-2004-NEST-C-1-028781) and Immunanomap Grant (MRTN-CT-2006-035946) of the European Union to C.G.F. I.Y.P and G.J.V. thank the Dutch Polymer Institute for financial support (DPI-695). A.C. and P.J. were supported by VENI Grants (916.66.028 and 700.57.401) of the Netherlands Organization for Scientific Research (NWO).

Appendix A

A.1. Protocol for AFM spring constant calibration

Preparation for experiments (all methods)

- Check *z*-calibration of your AFM, for instance using a calibration grid.
- Write down the temperature (°C) at the position of a mounted cantilever in a working AFM.
- Find the tilt angle off horizontal of the cantilever in its tip holder (e.g., see Table S1).
- Mount the cantilever into its holder, and align the laser-spot as close as possible to the end of the cantilever by a camera or microscope.
- Align the reflected laser beam onto the center of the photodetector and maximize the total intensity.

1. Thermal noise method

- Take force curves ($N=5$) of the cantilever in air on an ethanol cleaned silicon slide (or glass). Keep the deflection in the non-contact (flat) region at 0 V and the deflection in the contact region at a maximum of 1–2 V (<200 nm). Set the deflection set-point at 0 V.[3]
- Calculate the mean of the contact InvOLS (nm/V; sensitivity deflection) from the linear slope of the tip-sample contact region (in the approach curve). Enter this value in the software, if possible; and/or write it down.
- Raise the cantilever well above the substrate (>300 μm), without changing the laser position and re-center deflection to 0 V.[4]
- When possible, before acquiring the thermal noise data enter the measured InvOLS and temperature into the software. Also enter some correction parameters in your software to comply to Eq. (2); where $C=0.817$ for rectangular cantilevers, or $C=0.764$ for V-shaped cantilevers. (Note: The value you have to put into the software varies according the AFM system used, for NSs set the 'deflection sensitivity correction' to 1.106 or 1.144, other AFMs: check manual).
- Acquire the thermal noise power spectrum of the cantilever ($N=5$) and, if possible, save the spectrum for later analysis.

Calculating the spring constant:

- Fit the fundamental resonance peak in the spectrum with the SHO model.[5,6] Write down the fitting parameters y_0, A_0, f_R and Q of the SHO fit (Eq. (3)).
- Find the spring constant using the software, or manually calculate it with Eq. (5).

Calibration in liquid:

Alternative to calibrating in air, the thermal noise method can be applied in liquid. This implies that the InvOLS as well as the thermal noise should be acquired in this medium. Note that the InvOLS in liquid is related to that in air by the refractive index of that liquid, for further reading see [56]. Furthermore, due to higher damping, the signal-to-noise ratio is lower in the PSD. For highly damped systems, $Q \leq 10$, an adapted SHO fit should be used. For further reading on calibrating in liquid see [38].

2. Sader method
Before the calibration:

- Measure the plan-view dimensions of the cantilever by SEM or optical microscopy, and determine its length (L) and its width (b).

Calibration:

- Keep the cantilever well above the substrate (>300 μm), and set the deflection to 0 V.[3]
- Acquire the thermal noise power spectrum of the cantilever ($N=5$) and save the spectrum for later analysis.
- Fit the fundamental resonance peak with the SHO model. Write down the fitting parameters f_R and Q of the SHO fit (Eq. (3)).

[3] By calibrating at a ± 0 V deflection and a 0 V setpoint in the deflection versus piezo distance curves, the photodetector and piezo scanner both stay in their linear regime.

[4] The laser has shifted due to the change in electrostatic interaction of the cantilever with the substrate.

[5] In the thermal spectra also higher order peaks can be observed. Note that these can be 'false' peaks due to aliasing, which can be avoided by an anti-aliasing filter (see [32], for more information).

[6] A SHO fit is better than a Lorentz fit, which is sometimes implemented in the software of commercial AFM systems.

Alternative 1 (rectangular cantilever):

- Use the parameters f_R and Q to calculate the spring constant of a rectangular cantilever using Eqs. (6a) and (6b). Use the length L and width b of the cantilever as determined earlier. (For cantilever B from a MLCT/MSCT chip, take the values from Table 2). Take the temperature dependent values for ρ, η from Table S3 or use the calculator on: http://www.mhtl.uwaterloo.ca/old/onlinetools/airprop/airprop.html.
- Calculate the spring constant using Eq. (5), implemented in a self-written software application (e.g., in MATLAB) or use the web tool of the Sader group on: http://www.ampc.ms.unimelb.edu.au/afm/calibration.html.
- Correct the measured intrinsic spring constant for cantilever tilt with Eq. (8).

Alternative 2 (V-shaped cantilever C or D from a MLCT/MSCT-cantilever chip):

- Use the parameters f_R and Q to calculate the spring constant of V-shaped cantilevers C and D using Eq. (7a) and (7b), respectively. Thereby, calculate Re with Eq. (6b). Take the values for ρ, η, $b_{C/D}$, and $L_{C/D}$ from Table 2 and S3.
- Correct the found intrinsic spring constant for cantilever tilt with Eq. (8).

Alternative 3 (other V-shaped or differently shaped cantilevers):

- Derive alternative formulas for Eqs. (7a) and (7b), using the method described by Sader et al. in [30].
- After deriving the formulas, continue with **Alternative 2**.

Calibration in liquid:

The Sader method can be applied in liquid too (see also thermal noise method in liquid); the viscosity and density of water can be calculated on: http://www.mhtl.uwaterloo.ca/old/onlinetools/airprop/airprop.html.

Appendix B. Supplementary materials

Supplementary data associated with this article can be found in the online version at doi:10.1016/j.ultramic.2011.09.012.

References

[1] G. Binnig, C.F. Quate, C. Gerber, Atomic force microscope, Physical Review Letters 56 (1986) 930–933.
[2] P. Hinterdorfer, Y.F. Dufrene, Detection and localization of single molecular recognition events using atomic force microscopy, Nature Methods 3 (2006) 347–355.
[3] F. Oesterhelt, D. Oesterhelt, M. Pfeiffer, A. Engel, H.E. Gaub, D.J. Muller, Unfolding pathways of individual bacteriorhodopsins, Science 288 (2000) 143–146.
[4] E.L. Florin, V.T. Moy, H.E. Gaub, Adhesion forces between individual ligand–receptor pairs, Science 264 (1994) 415–417.
[5] V.T. Moy, E.L. Florin, H.E. Gaub, Intermolecular forces and energies between ligands and receptors, Science 266 (1994) 257–259.
[6] M. Rief, H. Clausen-Schaumann, H.E. Gaub, Sequence-dependent mechanics of single DNA molecules, Nature Structural and Molecular Biology 6 (1999) 346–349.
[7] K.O. Greulich, Single-molecule studies on DNA and RNA, ChemPhysChem 6 (2005) 2458–2471.
[8] P. Frederix, P.D. Bosshart, A. Engel, Atomic force microscopy of biological membranes, Biophysical Journal 96 (2009) 329–338.
[9] M. Rief, M. Gautel, F. Oesterhelt, J.M. Fernandez, H.E. Gaub, Reversible unfolding of individual titin immunoglobulin domains by AFM, Science 276 (1997) 1109–1112.
[10] M.I. Giannotti, G.J. Vancso, Interrogation of single synthetic polymer chains and polysaccharides by AFM-based force spectroscopy, ChemPhysChem 8 (2007) 2290–2307.
[11] M. Grandbois, M. Beyer, M. Rief, H. Clausen-Schaumann, H.E. Gaub, How strong is a covalent bond? Science 283 (1999) 1727–1730.
[12] S. Zou, H. Schönherr, G.J. Vancso, Force spectroscopy of quadruple H-bonded dimers by AFM: dynamic bond rupture and molecular time-temperature superposition, Journal of the American Chemical Society 127 (2005) 11230–11231.
[13] M. Benoit, D. Gabriel, G. Gerisch, H.E. Gaub, Discrete interactions in cell adhesion measured by single-molecule force spectroscopy, Nature Cell Biology 2 (2000) 313–317.
[14] J. Helenius, C.P. Heisenberg, H.E. Gaub, D.J. Muller, Single-cell force spectroscopy, Journal of Cell Science 121 (2008) 1785–1791.
[15] S.K. Kufer, E.M. Puchner, H. Gumpp, T. Liedl, H.E. Gaub, Single-molecule cut-and-paste surface assembly, Science 319 (2008) 594–596.
[16] H.G. Hansma, K.J. Kim, D.E. Laney, R.A. Garcia, M. Argaman, M.J. Allen, S.M. Parsons, Properties of biomolecules measured from atomic force microscope images: a review, Journal of Structral Biology 119 (1997) 99–108.
[17] R. Garcia, R. Perez, Dynamic atomic force microscopy methods, Surface Science Reports 47 (2002) 197–301.
[18] C.A. Clifford, M.P. Seah, The determination of atomic force microscope cantilever spring constants via dimensional methods for nanomechanical analysis, Nanotechnology 16 (2005) 1666–1680.
[19] J.M. Neumeister, W.A. Ducker, Lateral, normal, and longitudinal spring constants of atomic-force microscopy cantilevers, Review of Scientific Instruments 65 (1994) 2527–2531.
[20] J.E. Sader, L. White, Theoretical-analysis of the static deflection of plates for atomic-force microscope applications, Journal of Applied Physics 74 (1993) 1–9.
[21] Y.Q. Li, N.J. Tao, J. Pan, A.A. Garcia, S.M. Lindsay, Direct measurement of interaction forces between colloidal particles using the scanning force microscope, Langmuir 9 (1993) 637–641.
[22] Y.I. Rabinovich, R.H. Yoon, Use of atomic-force microscope for the measurements of hydrophobic forces between silanated silica plate and glass sphere, Langmuir 10 (1994) 1903–1909.
[23] A. Torii, M. Sasaki, K. Hane, S. Okuma, A method for determining the spring constant of cantilevers for atomic force microscopy, Measurement Science and Technology 7 (1996) 179–184.
[24] S.K. Jericho, M.H. Jericho, Device for the determination of spring constants of atomic force microscope cantilevers and micromachined springs, Review of Scientific Instruments 73 (2002) 2483–2485.
[25] K.H. Chung, S. Scholz, G.A. Shaw, J.A. Kramar, J.R. Pratt, SI traceable calibration of an instrumented indentation sensor spring constant using electrostatic force, Review of Scientific Instruments 79 (2008) 095105.
[26] E.D. Langlois, G.A. Shaw, J.A. Kramar, J.R. Pratt, D.C. Hurley, Spring constant calibration of atomic force microscopy cantilevers with a piezosensor transfer standard, Review of Scientific Instruments 78 (2007) 10.
[27] J.P. Cleveland, S. Manne, D. Bocek, P.K. Hansma, A nondestructive method for determining the spring constant of cantilevers for scanning force microscopy, Review of Scientific Instruments 64 (1993) 403–405.
[28] J.L. Hutter, J. Bechhoefer, Calibration of atomic-force microscope tips, Review of Scientific Instruments 64 (1993) 1868–1873.
[29] J.E. Sader, J.W.M. Chon, P. Mulvaney, Calibration of rectangular atomic force microscope cantilevers, Review of Scientific Instruments 70 (1999) 3967–3969.
[30] J.E. Sader, J. Pacifico, C.P. Green, P. Mulvaney, General scaling law for stiffness measurement of small bodies with applications to the atomic force microscope, Journal of Applied Physics 97 (2005) 1249031–1249037.
[31] B. Ohler, Cantilever spring constant calibration using laser Doppler vibrometry, Review of Scientific Instruments 78 (2007) 0637011–0637015.
[32] S. Cook, T.E. Schaffer, K.M. Chynoweth, M. Wigton, R.W. Simmonds, K.M. Lang, Practical implementation of dynamic methods for measuring atomic force microscope cantilever spring constants, Nanotechnology 17 (2006) 2135–2145.
[33] B. Ohler, Practical advice on the determination of cantilever spring constants, Veeco Instrum. Inc. Internal Publ., 2007, pp. 1–12.
[34] N.A. Burnham, X. Chen, C.S. Hodges, G.A. Matei, E.J. Thoreson, C.J. Roberts, M.C. Davies, S.J.B. Tendler, Comparison of calibration methods for atomic-force microscopy cantilevers, Nanotechnology 14 (2003) 1–6.
[35] C.T. Gibson, D.A. Smith, C.J. Roberts, Calibration of silicon atomic force microscope cantilevers, Nanotechnology 16 (2005) 234–238.
[36] H.J. Butt, M. Jaschke, Calculation of thermal noise in atomic-force microscopy, Nanotechnology 6 (1995) 1–7.
[37] R.W. Stark, T. Drobek, W.M. Heckl, Thermomechanical noise of a free V-shaped cantilever for atomic-force microscopy, Ultramicroscopy 86 (2001) 207–215.
[38] T. Pirzer, T. Hugel, Atomic force microscopy spring constant determination in viscous liquids, Review of Scientific Instruments 80 (2009) 035110.
[39] C.T. Gibson, D.J. Johnson, C. Anderson, C. Abell, T. Rayment, Method to determine the spring constant of atomic force microscope cantilevers, Review of Scientific Instruments 75 (2004) 565–567.
[40] R. Proksch, T.E. Schaffer, J.P. Cleveland, R.C. Callahan, M.B. Viani, Finite optical spot size and position corrections in thermal spring constant calibration, Nanotechnology 15 (2004) 1344–1350.
[41] T.E. Schaffer, Calculation of thermal noise in an atomic force microscope with a finite optical spot size, Nanotechnology 16 (2005) 664–670.

[42] D.A. Walters, J.P. Cleveland, N.H. Thomson, P.K. Hansma, M.A. Wendman, G. Gurley, V. Elings, Short cantilevers for atomic force microscopy, Review of Scientific Instruments 67 (1996) 3583–3590.
[43] J.W.M. Chon, P. Mulvaney, J.E. Sader, Experimental validation of theoretical models for the frequency response of atomic force microscope cantilever beams immersed in fluids, Journal of Applied Physics 87 (2000) 3978–3988.
[44] J.E. Sader, Frequency response of cantilever beams immersed in viscous fluids with applications to the atomic force microscope, Journal of Applied Physics 84 (1998) 64–76.
[45] J.L. Hutter, Comment on tilt of atomic force microscope cantilevers: effect on spring constant and adhesion measurements, Langmuir 21 (2005) 2630–2632.
[46] W.C. Young, R.G. Budynas, R.J. Roark, Roark's Formulas for Stress and Strain , 2001.
[47] J.E. Sader, Parallel beam approximation for V-shaped atomic-force microscope cantilevers, Review of Scientific Instruments 66 (1995) 4583–4587.
[48] J.E. Sader, I. Larson, P. Mulvaney, L.R. White, Method for the calibration of atomic-force microscope cantilevers, Review of Scientific Instruments 66 (1995) 3789–3798.
[49] J.L. Hazel, V.V. Tsukruk, Spring constants of composite ceramic/gold cantilevers for scanning probe microscopy, Thin Solid Films 339 (1999) 249–257.
[50] G.I. Bell, Models for the specific adhesion of cells to cells, Science 200 (1978) 618–627.
[51] E. Evans, K. Ritchie, Dynamic strength of molecular adhesion bonds, Biophysical Journal 72 (1997) 1541–1555.
[52] D.F. Tees, R.E. Waugh, D.A. Hammer, A microcantilever device to assess the effect of force on the lifetime of selectin-carbohydrate bonds, Biophysical Journal 80 (2001) 668–682.
[53] P. Panorchan, M.S. Thompson, K.J. Davis, Y. Tseng, K. Konstantopoulos, D. Wirtz, Single-molecule analysis of cadherin-mediated cell–cell adhesion, Journal of Cell Science 119 (2006) 66–74.
[54] J. te Riet, A.W. Zimmerman, A. Cambi, B. Joosten, S. Speller, R. Torensma, F.N. van Leeuwen, C.G. Figdor, F. de Lange, Distinct kinetic and mechanical properties govern ALCAM-mediated interactions as shown by single molecule force spectroscopy, Journal of Cell Science 120 (2007) 3965–3976.
[55] M.J. Higgins, R. Proksch, J.E. Sader, M. Polcik, S. Mc Endoo, J.P. Cleveland, S.P. Jarvis, Noninvasive determination of optical lever sensitivity in atomic force microscopy, Review of Scientific Instruments 77 (2006) 013701–013705.
[56] E. Tocha, J. Song, H. Schonherr, G.J. Vancso, Calibration of friction force signals in atomic force microscopy in liquid media, Langmuir 23 (2007) 7078–7082.